Image Denoising with Recurrent Polak-Ribière-Polyak Conjugate Gradient-Based Neuro-Fuzzy Edge-Preserving Segmentation Based on OAMNHA

K. Indupriya, Anna Saro Vijendran

***Abstract*: *The most essential process in image processing applications is eliminating the noisy pixels from the images and acquiring the noise-free images with better reconstructed quality. This process has high complexity due to the segmentation of image patches from the noisy images. To simplify this process, Neuro-Fuzzy filtering with Optimum Adaptive parameterized Mask Non-Harmonic Analysis in Curvelet Transform domain (NF-OAMNHA-CT) has been proposed for image denoising. It uses NF edge detector instead of canny edge detector for segmenting and preserving the edge regions including homogeneous texture boundaries with minimized edge distortion. However, it requires gradient information about the error function with respect to the parameter measures during training of NF for optimizing their parameters. Also, it often affects with the fixed local minima. Therefore in this article, Recurrent Polak- Ribière-Polyak Conjugate Gradient-Based Neuro-Fuzzy (RPCGNF-OAMNHA-CT) technique is proposed to enhance the edge-preserving segmentation in image denoising. At first, the noisy images are defined in the CT domain and fed to the RPCGNF edge detector as edge-preserving segmentation that segments and extracts the edge regions as well as homogeneous texture regions. In this RPCGNF technique, recurrent mechanism is applied to construct PCGNF as an updated edge-preserving segmentation technique that learns their parameters with high efficiency and speeding up the convergence. As a result, the edge regions and homogeneous textures are synchronously segmented as noisy pixels until either the PCGNF converges to the desired accuracy of segmentation or a termination criterion is reached. Further, OAMNHA is applied on each segment to remove the noisy pixels from the images and obtain the noise-free images accurately. Finally, the experimental results illustrate the proposed RPCGNF-OAMNHA-CT technique achieves higher efficiency than the NF-OAMNHA-CT technique in terms of Peak Signal-to-Noise Ratio (PSNR), Mean Absolute Error (MAE) and Structural Similarity (SSIM).*

Index Terms*: *Image denoising, Edge-preserving segmentation, NF-OAMNHA-CT, Polak-Ribière-Polyak Conjugate Gradient method, Recurrent mechanism, Convergence

I. INTRODUCTION

Digital images are normally affected by noise during capturing and transmitting them from one location to another through wired or wireless channels. In the field of image processing and computer vision, image denoising is one of the most critical challenges since the main aim is estimating the underlying image by eliminating the noise from the noisy images. A foremost challenge is eliminating the noise as much as promising without removing the most representative features of the image like edges, corners and other pointed structures. To tackle this challenge, Hosotani et al. [1] proposed a Mask Non-Harmonic Analysis (M-NHA) for achieving image denoising with edge preserving and segmentation. In this technique, a high resolution frequency analysis was used to remove the zero-mean white Gaussian noise. Besides, M-NHA was used to analyze the non-uniform regions found out by the segmentation process that increases the Peak Signal-to-Noise Ratio (PSNR). On the other hand, optimizing the parameters used in the segmentation process was not effective and suppressing the irrelevant data during edge detection process was achieved by predetermined threshold value.

As a result, an Optimum Adaptive parameterized M-NHA (OAMNHA)-based image denoising technique was suggested that uses Support Vector Machine (SVM) and firefly optimization algorithms [2]. In this technique, SVM was applied to learn the parameters employed in the segmentation process and firefly algorithm was applied to optimize the threshold values for different noisy images. Conversely, the effectiveness of denoising process was relied on the homogeneous texture segmentation because it utilizes the feature vectors in spatial domain which are not considered to search similar patches from arbitrary regions. For this reason, the frequency domain coefficients were used for segmentation [3]. To achieve this, the spatial domain image was converted into different frequency domains independently. Those were named as OAMNHA-WT (Wavelet Transform), OAMNHA-CoT (Contourlet Transform) and OAMNHA-CT (Curvelet Transform). After that, the image was decomposed as many subband images and then the segmentation process was performed in which the computed frequency coefficients were used to discover the homogeneous patches. Finally, 2D-NHA and inverse frequency transforms were carried out separately to fuse all subband images. Among them, OAMNHA-CT technique can effectively eliminate the noisy pixels from the image through segmentation process.

Revised Manuscript Received on November 05, 2019.

K. Indupriya, Research Scholar, Department of Computer Science, Sri Ramakrishna College of Arts and Science, Coimbatore, Tamilnadu, India. Email: indupriya1406@gmail.com

Dr. Anna Saro Vijendran, Dean, School of Computing, Sri Ramakrishna College of Arts and Science College, Coimbatore, Tamilnadu, India. Email: saroviji@rediffmail.com

But, it has complex to determine the region boundary in the noisy image. In these techniques, the segmentation has fuzziness in the decision of the region boundary. It was believed that these fuzzy boundaries have to be termed as edge regions. So, canny edge detector was applied to detect the edge points with homogeneous textures. Conversely, this detector has high computational complexity and thus it was time-consuming. To solve this problem, a Neuro-Fuzzy (NF)-based edge detector was proposed as an edge-preserving segmentation method with OAMNHA-CT technique [4]. In this NF-OAMNHA-CT technique, the image was given to the NF edge detector for classification of whether the pixel was edge pixel or not. This process was continued for all the pixels to extract the edges in the noisy images. The extracted edges were represented as the region boundaries i.e., edge regions. As well, homogeneous texture segmentation was performed to create the texture boundaries. Moreover, Levenberg–Marquardt (LM) optimization algorithm was used for tuning the internal parameters of NF edge detector. At last, each segment was applied to the OAMNHA for reconstructing the noise-free images. Though it reduces the time consumption of detecting edge regions, LM optimization algorithm for parameter tuning needs gradient information about the error function with respect to the parameter estimates and frequently affects by the fixed local minima.

Hence in this article, Recurrent Polak-Ribière-Polyak Conjugate Gradient-Based Neuro-Fuzzy (RPCGNF-OAMNHA-CT) technique is proposed. In this technique, the NF is trained by RPCG-based algorithm that efficiently enhances the learning performance. This recurrent technique can execute filtering noisy pixels for constructing PCGNF technique as an updated edge-preserving segmentation for segmenting the noisy pixels synchronously until either this PCGNF converges to the desired accuracy or a termination criterion is reached. Thus, the parameters of NF are learned efficiently than the standard gradient methods in terms of effectiveness and speeding up the convergence. Also, it can obtain more useful convergence results which can efficiently support the real-time image denoising applications.

The remaining part of this article is prepared as follows: Section II reviews the previous researches related to the image denoising techniques. Section III describes the methodology of proposed RPCGNF-OAMNHA-CT technique. Section IV analyzes the performance of RPCGNF-OAMNHA-CT technique and compares with the existing techniques. Section V concludes the research work.

II. LITERATURE SURVEY

Wang et al. [5] proposed a novel denoising technique based on Non-Subsampled Shearlet Transform (NSST) and Fuzzy Support Vector Machines (FSVMs) that suppresses the noise from an image when preserving its features. Initially, the noisy image was decomposed into many subbands of frequency and orientation responses using NSST. Then, the NSST detail coefficients were split into edge/texture-related and noise-related coefficients by using FSVM classifier. At last, the detail subbands of NSST coefficients were denoised by the adaptive Bayesian threshold. However, the computational complexity of this technique was high.

Fu et al. [6] proposed a novel despeckling algorithm for enhancing the image quality of medical ultrasound images. In this algorithm, coefficients in the Dual-Tree Complex Wavelet Transform (DTCWT) domain was used for enhancing a novel quantum-inspired thresholding function. The inter-scale correlation among the coefficients of many subbands and the intra-scale variance between the coefficient and its neighborhood in similar subband were used for developing a novel thresholding function. Then, this function was integrated in the Bayesian network for achieving an adaptive image despeckling. However, SNR was not effective.

Abdallah et al. [7] proposed a novel Adaptive Noise-Reducing Anisotropic Diffusion (ANRAD) technique for improving the image quality by using a modified Speckle-Reducing Anisotropic Diffusion (SRAD) filter. In this technique, an automatic RGB noise model estimator was introduced to estimate an upper bound of the real noise level function at each iteration by fitting a lower envelope to the standard deviations of pre-segment image variations. However, the computational time complexity was high and it does not perform well for images with textures.

Xu et al. [8] proposed a noise removal technique based on a semi-adaptive threshold in anisotropic diffusion filter for achieving better detail information preservation and stronger noise suppressing ability. In this technique, a method of local variance rate was applied for differentiating the corrupted pixels and noise-free pixels. Also, the parts of the corrupted pixels were restored by the pixels which have been pre-denoised via a Gaussian filter. After that, an anisotropic diffusion model with a semi-adaptive threshold in diffusion coefficient function was applied for obtaining the restored image. Moreover, the gradient value of the corrupted pixels was applied in the semi-adaptive threshold for providing a high diffusion in smooth regions and less diffusion in edge regions. However, the efficiency of pre-reduction of noise was less.

Rafsanjani et al. [9] proposed an algorithm that adaptively chooses diffusion coefficient using the residual local power and the number of the gradient magnitude. In this algorithm, a texture detector operator was introduced by applying Perona and Malik (PM) process to the noisy image and computing the local variations of residue. The residual local variation was adaptively scaled during the time and inserted to the diffusion coefficient argument of PM model to control it. However, the computational complexity was high.

Fedorov & Ballester [10] proposed an enhanced non-local means denoising method for effectively achieving the affine invariant self-similarities present in the real-scene images. In this method, an affine invariant patch similarity measure was used that performs an appropriate patch comparison by automatically and intrinsically adapting the size and shape of the patches. Therefore, more similar patches were discovered and appropriately used for denoising of the images. But, the performance may suffer from over-smoothing in some cases.

Shahdoosti & Hazavei [11] proposed a novel Hidden Markov Tree (HMT) model for image denoising. Initially, HMT with the fusion of one-sided exponential densities for considering the signs of transform coefficients during image denoising. Then, a novel efficient model was constructed by two one-sided exponential densities and one Gaussian density. Also, this method utilizes the Dual Contourlet Transform (DCT) formed by the mixture of the Directional Filter Bank (DFB) and the DTCWT. However, computation time was high.

Guo et al. [12] proposed a new edge-preserving image denoising algorithm that reconstructs both low and high frequency components of the image independently. In this algorithm, a neighbourhood regression scheme was proposed for restoring the high frequency components. Also, an energy minimization function was used to fuse the low and high frequency components for restoring the denoised image. On the other hand, this algorithm has high average runtime.

III. PROPOSED METHODOLOGY

In this section, the proposed RPCGNF-OAMNHA-CT-based image denoising technique is described in brief. The flow diagram of RPCGNF-OAMNHA-CT technique is shown in Fig. 1. At first, an image $i(x, y)$ with size $M \times N$ is converted to the CT coefficients. After that, the transformed image is fed to the PCGNF edge detector with recurrent mechanism for segmenting both edge and homogeneous texture regions as follows:

Consider $\{x^j, o^j\}_{j=1}^{J} \subset \mathbb{R}^m \times \mathbb{R}$ is the training image that will be used for training the zero-order Takagi-Sugeno (TS) NF system shown in Fig. 2. The key fuzzy rule base for the system is determined by rules of the form:

$$Rule\ i\ (R_i): IF\ x_1\ is\ A_{1i}\ and\ x_2\ is\ A_{2i}\ and\ \dots and\ x_m\ is\ A_{mi},\ THEN\ y\ is\ y_i, i = 1,2,\dots,n$$

Here, i is the i^{th} fuzzy rule, n is the total number of fuzzy rules, y_i is the real number, A_{li} is the fuzzy subset of x_l computed by using a Gaussian membership function as:

$$A_{li}(x_l) = e^{\left(-(x_l - a_{li})^2 / \sigma_{li}^2\right)} \quad (1)$$

In Eq. (1), a_{li} and σ_{li} are the centroid and the size of $A_{li}(x_l)$, respectively.

Consider $a_0 = (y_1, y_2, \dots, y_n)$ is the output layer weight vector linking Layer 3 i.e., rule layer and Layer 4 i.e., output layer. As well, $a_i = (a_{1i}, a_{2i}, \dots, a_{mi})$ is defined as the centroids of the corresponding Gaussian membership functions. The singularity in computing the derivatives is avoided by defining the reciprocals of sizes as: $b_i = (b_{1i}, b_{2i}, \dots, b_{mi}) = \left(\frac{1}{\sigma_{1i}}, \frac{1}{\sigma_{2i}}, \dots, \frac{1}{\sigma_{mi}}\right)$ where $1 \le i \le n$. Both a_i and b_i act as the input weight vectors which link the Layer 1 i.e., input layer and Layer 2 i.e., membership layer.

For simplification, a_0 and a_i are combined with b_i ($i = 1,2,\dots,n$ and the combined weight vector is denoted as $w = (a_0, a_1, \dots, a_n, b_1, \dots, b_n) \in \mathbb{R}^{(2m+1)n}$. The error function of the NF network is defined as follows:

$$E(w) = \frac{1}{2}\sum_{j=1}^{J}(y^j - o^j)^2 = \sum_{j=1}^{J} g_j(a_0 \cdot h^j) \quad (2)$$

In Eq. (2), J denotes the total number of training samples, y^j denotes the actual output computed by the NF network for the j^{th} given input x^j and o^j is the corresponding target output. Also,

$$h^j = \left(h_1^j, h_2^j, \dots, h_i^j\right) = h(x^j), g_j(t) = \frac{1}{2}(t - o^j)^2 \quad (3)$$

Where $1 \le j \le J, t \in \mathbb{R}$

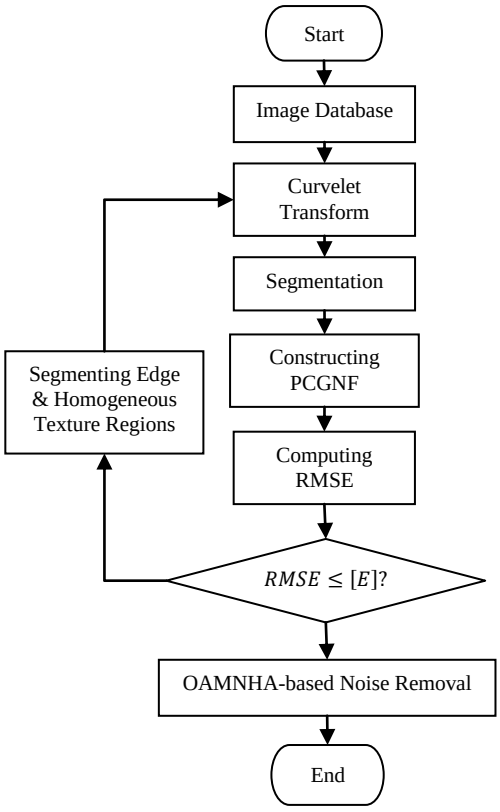

Fig. 1: Flow Diagram of RPCGNF-OAMNHA-CT-based Image Denoising

In Eq. (3), h_i^j denotes the firing strength of the i^{th} rule for the j^{th} input vector. The aim of RPCGNF training is finding the best weight vector (w^*) that optimizes the error function defined in Eq. (2) i.e., $E(w^*) = \min E(w)$ and this problem is solved by using conjugate gradient methods. By using $b_{li} = \frac{1}{\sigma_{li}};\ \sigma_{li} \neq 0$, obtain

$$A_{li}(x_l) = e^{(-(x_l - a_{li})^2 b_{li}^2)}, l = 1,2,\dots,m; i = 1,2,\dots,n \quad (4)$$

Therefore, the firing strength of the i^{th} rule in Layer 3 i.e., rule layer is computed by using the softmin as:

$$h_q^j = \left(\sum_{l=1}^{m} A_{lq}\left(x_l^j\right) e^{\beta A_{lq}\left(x_l^j\right)}\right) \Big/ \left(\sum_{l=1}^{m} e^{\beta A_{lq}\left(x_l^j\right)}\right), \quad (5)$$

In Eq. (5), $j = 1, \dots, J; q = 1,2,\dots,n$, $A_{lq}\left(x_l^j\right) = e^{\left(-\left(x_l^j - a_{lq}\right)^2 b_{lq}^2\right)}$ and β denotes the constant.

The following simple terms are defined for simplification:

$$E_w^k = E_w(w^k), E_{a_0}^k = E_{a_0}(w^k) \quad (6)$$

$$E_{a_i}^k = E_{a_i}(w^k), E_{b_i}^k = E_{b_i}(w^k) \quad (7)$$

In Eq. (6) & (7), k ($k \in \mathbb{N}$) is the index of the network training iterations. Initializing with an arbitrary primary weight w^0, the weight vector w is updated iteratively by the following terms:

$$w^{k+1} = w^k + \eta d^k, d^k = -E_w^k + \gamma^k d^{k-1} \quad (8)$$

In Eq. (8), $\eta > 0$ denotes the step size for learning.

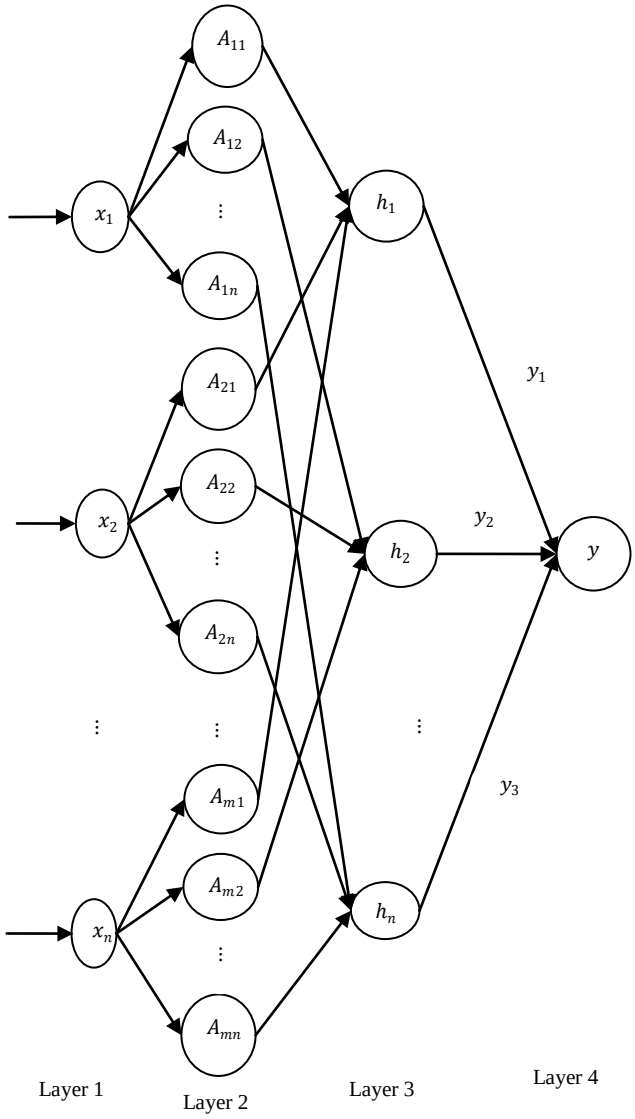

Fig. 2: Structure of Zero-order TS NF System

$$\gamma^k = \begin{cases} 0, & k = 0 \\ \frac{(E_w^k)^T (E_w^k - E_w^{k-1})}{\|E_w^{k-1}\|^2}, & k \geq 1 \end{cases} \quad (9)$$

$$d^{-1} = 0 \quad (10)$$

Based on Eq. (2) and $w = (a_0, a_1, \dots, a_n, b_1, \dots, b_n) \in \mathbb{R}^{(2m+1)n}$, the gradient term is defined as:

$$E_w(w) = \left(E_{a_0}(w), E_{a_1}(w), \dots, E_{a_n}(w), E_{b_1}(w), \dots, E_{b_n}(w)\right) \quad (11)$$

Where $E_{a_0}(w) = \sum_{j=1}^{J} g_j'(a_0 \cdot h^j) h^j$

To calculate the gradient $E_{a_i}(w)$, consider,

$$c_i = (c_{1i}, c_{2i}, \dots, c_{mi}) = \left(\frac{A_{1i}(x_1^j)\left(1+\beta A_{1i}(x_1^j)\right)e^{\beta A_{1i}(x_1^j)}}{\sum_{l=1}^{m} A_{li}(x_l^j) e^{\beta A_{li}(x_l^j)}} - \frac{\beta A_{1i}(x_1^j) e^{\beta A_{1i}(x_1^j)}}{\sum_{l=1}^{m} e^{\beta A_{li}(x_l^j)}}, \frac{A_{2i}(x_2^j)\left(1+\beta A_{2i}(x_2^j)\right)e^{\beta A_{2i}(x_2^j)}}{\sum_{l=1}^{m} A_{li}(x_l^j) e^{\beta A_{li}(x_l^j)}} - \frac{\beta A_{2i}(x_2^j) e^{\beta A_{2i}(x_2^j)}}{\sum_{l=1}^{m} e^{\beta A_{li}(x_l^j)}}, \dots, \frac{A_{mi}(x_m^j)\left(1+\beta A_{mi}(x_m^j)\right)e^{\beta A_{mi}(x_m^j)}}{\sum_{l=1}^{m} A_{li}(x_l^j) e^{\beta A_{li}(x_l^j)}} - \frac{\beta A_{mi}(x_m^j) e^{\beta A_{mi}(x_m^j)}}{\sum_{l=1}^{m} e^{\beta A_{li}(x_l^j)}} \right) \quad (12)$$

By using Eq. (5) & (12),

$$\frac{\partial h_q^j}{\partial a_i} = \begin{cases} 0, & \forall q \neq i \\ 2h_i^j (x^j - a_i) \odot b_i \odot b_i \odot c_i, & \forall q = i \end{cases} \quad (13)$$

Based on Eq. (2) & (13), the gradient $E_{a_i}(w)$ is rewritten as:

$$E_{a_i}(w) = \sum_{j=1}^{J} g_j'(a_0 \cdot h^j) \left(\sum_{q=1}^{n} y_q \frac{\partial h_q^j}{\partial a_i} \right)$$

$$= 2\sum_{j=1}^{J} g_j'(a_0 \cdot h^j)\, h_i^j y_i \left((x^j - a_i) \odot b_i \odot b_i \odot c_i\right) \quad (14)$$

Similarly, for $1 \leq i \leq n$, the gradient $E_{b_i}(w)$ is written as:

$$E_{b_i}(w) = -2\sum_{j=1}^{J} g_j'(a_0 \cdot h^j)\, h_i^j y_i \times \left((x^j - a_i) \odot (x^j - ai \odot bi \odot ci \right) \quad (15)$$

Then, convergence analysis is conducted based on the following basic hypotheses:

- The first derivative of $g(t), g'(t)\ (t \in \mathbb{R})$ is local Lipschitz continuous and denote $L > 0$ as the Lipschitz constant;
- The weight sequence is equally bounded i.e., $\|w^k\| \leq C_0$ where C_0 denotes the positive constant, $k \in \mathbb{N}$;
- For a compact set D_0, the stationary set $\Omega = \{w \in D_0 : E_w(w) = 0\}$ has a finite number of points.

Moreover, it is required to indicate the following constants for the ease of convergence analysis:

$$M = \max_{1 \leq j \leq J} \{\|x^j\|, \|o^j\|\} \quad (16)$$

$$C_1 = \max\{C_0 + M, (C_0 + M)C_0\} \quad (17)$$

Thus, this process is repeated for removing all noisy pixels in the images accurately. Therefore, the edge and texture regions are segmented independently which are fed to the OAMNHA for reconstructing the noiseless images with minimum computational complexity and maximum accuracy.

IV. RESULTS AND DISCUSSIONS

In this section, the performance analysis of proposed RPCGNF-OAMNHA-CT-based image denoising technique is evaluated using MATLAB 2018a and compared with the NF-OAMNHA-CT technique in terms of PSNR, SSIM and MAE. In this evaluation, the target images with various features are gathered from the Laboratory for Image Video Engineering (LIVE) image database at the University of Texas at Austin [13]. The results of proposed RPCGNF-OAMNHA-CT based image denoising technique are shown in Fig. 3.

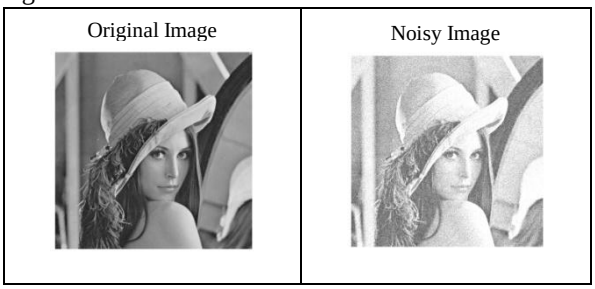

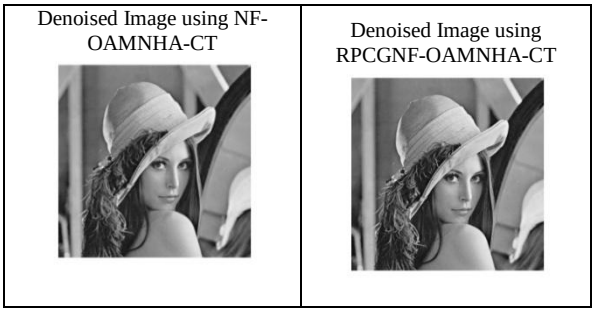

Fig.3 Results of Proposed and Existing Denoising Technique for Lena Image

A. PSNR

It defines the fraction of the most probable power of image (signal) to the power of the corrupting noise that affects the image quality.

$$PSNR = 10\log_{10}\frac{255^2}{MSE} \quad (18)$$

$$\text{Where } MSE = \frac{1}{M\times N}\sum_{x=1}^{M-1}\sum_{y=1}^{N-1}\left(i_{xy} - \hat{\imath}_{xy}\right)^2 \quad (19)$$

In Eq. (19), $M \times N$ is image size, i_{xy} and $\hat{\imath}_{xy}$ are the actual and denoised images, respectively. Table 1 shows the comparison of denoising PSNR under different noise densities (σ) for RPCGNF-OAMNHA-CT and NF-OAMNHA-CT techniques.

Table 1: Comparison of Denoising PSNR

σ	Cameraman		Bikes	
	NF-OAMNHA-CT	RPCGNF-OAMNHA-CT	NF-OAMNHA-CT	RPCGNF-OAMNHA-CT
5	46.25	48.44	46.62	48.87
10	45.21	47.63	42.86	44.62
15	41.38	43.85	41.03	43.75
20	40.48	42.52	38.55	40.91
25	39.06	41.76	37.39	39.24
30	38.13	40.19	36.72	38.03
σ	Ocean		Statue	
	NF-OAMNHA-CT	RPCGNF-OAMNHA-CT	NF-OAMNHA-CT	RPCGNF-OAMNHA-CT
5	48.03	50.36	48.05	50.91
10	43.49	45.72	43.61	45.84
15	42.99	44.51	42.89	44.63
20	40.11	42.93	41.33	43.55
25	38.62	40.65	38.74	40.47
30	37.85	39.84	37.92	39.79
σ	Barbara		Lena	
	NF-OAMNHA-CT	RPCGNF-OAMNHA-CT	NF-OAMNHA-CT	RPCGNF-OAMNHA-CT
5	47.68	49.81	48.86	50.99
10	44.21	46.57	44.37	46.56
15	41.19	43.69	43.22	45.48
20	40.06	42.45	42.31	44.67
25	38.34	40.38	41.95	43.85
30	37.95	39.73	39.04	41.31
σ	Coinsfountain		Lighthouse	
	NF-OAMNHA-CT	RPCGNF-OAMNHA-CT	NF-OAMNHA-CT	RPCGNF-OAMNHA-CT
5	46.28	48.66	47.68	49.81
10	43.51	45.94	42.31	44.65
15	40.85	42.37	41.85	43.33
20	38.43	40.59	38.47	40.76
25	38.36	40.29	37.52	39.92
30	36.74	38.48	37.19	39.04
σ	Stream			
	NF-OAMNHA-CT		RPCGNF-OAMNHA-CT	
5	43.06		45.62	
10	39.65		41.88	
15	38.71		40.53	
20	36.34		38.71	
25	43.87		45.34	
30	43.43		45.97	

Table 1 shows that the RPCGNF-OAMNHA-CT-based image denoising technique achieves higher PSNR compared with the NF-OAMNHA-CT technique. For example, when the statue with $\sigma = 5$ is considered for analysis, the PSNR of RPCGNF-OAMNHA-CT technique is 5.95% increased than the NF-OAMNHA-CT technique.

B. MAE

It refers to the absolute error between the actual image and the denoised image acquired after applying RPCGNF-OAMNHA-CT technique.

$$MAE = \frac{1}{M\times N}\sum_{x=1}^{M-1}\sum_{y=1}^{N-1}\left(i_{xy} - \hat{\imath}_{xy}\right) \quad (20)$$

Table 2 shows the comparison of denoising MAE under different σ for RPCGNF-OAMNHA-CT and NF-OAMNHA-CT techniques.

Table 2: Comparison of Denoising MAE

σ	Cameraman		Bikes	
	NF-OAMNHA-CT	RPCGNF-OAMNHA-CT	NF-OAMNHA-CT	RPCGNF-OAMNHA-CT
5	1.12	0.86	1.24	0.97
10	1.96	1.54	3.18	2.82
15	2.91	2.49	4.36	3.95
20	3.73	3.35	5.49	5.04
25	5.05	4.78	6.93	6.51
30	5.17	4.89	8.01	7.69
σ	Ocean		Statue	
	NF-OAMNHA-CT	RPCGNF-OAMNHA-CT	NF-OAMNHA-CT	RPCGNF-OAMNHA-CT
5	1.35	1.08	1.43	1.11
10	2.47	2.15	2.46	2.18
15	3.39	3.07	3.33	2.97
20	3.71	3.43	4.09	3.75
25	4.56	4.26	4.75	4.39
30	5.12	4.84	5.27	4.83
σ	Barbara		Lena	
	NF-OAMNHA-CT	RPCGNF-OAMNHA-CT	NF-OAMNHA-CT	RPCGNF-OAMNHA-CT
5	1.68	1.32	1.53	1.26
10	2.71	2.44	2.38	2.01
15	3.43	3.15	2.91	2.64
20	4.16	3.79	3.54	3.29
25	4.72	4.43	3.87	3.53
30	5.45	5.16	4.29	3.95
σ	Coinsfountain		Lighthouse	
	NF-OAMNHA-CT	RPCGNF-OAMNHA-CT	NF-OAMNHA-CT	RPCGNF-OAMNHA-CT
5	2.08	1.86	1.73	1.38
10	3.42	3.11	2.86	2.45
15	4.67	4.28	3.74	3.37
20	5.71	5.43	4.51	4.16
25	6.64	6.27	5.49	5.09
30	7.53	7.24	5.52	5.14
σ	Stream			
	NF-OAMNHA-CT		RPCGNF-OAMNHA-CT	
5	2.76		2.38	
10	5.04		4.67	
15	6.88		6.43	
20	8.25		7.86	
25	9.41		9.05	
30	10.53		10.14	

Table 2 shows that the RPCGNF-OAMNHA-CT-based image denoising technique reduces MAE compared with the NF-OAMNHA-CT technique.

C. SSIM

It refers to the similarity measure between two images $i_1(x,y)$ and $i_2(x,y)$.

$$SSIM(i_1,i_2)=\frac{(2\mu_{i_1}\mu_{i_2}+c_1)(2\sigma_{i_1i_2}+c_2)}{\left(\mu_{i_1}^2+\mu_{i_2}^2+c_1\right)\left(\sigma_{i_1}^2+\sigma_{i_2}^2+c_2\right)} \qquad (21)$$

In Eq. (21), μ_{i_1} and μ_{i_2} are the mean of i_1 and i_2, σ_{i_1} and σ_{i_2} are the variances of i_1 and i_2, c_1 and c_2 are constants and $\sigma_{i_1i_2}$ is the covariance of i_1 and i_2, respectively. Table 3 shows the comparison of denoising SSIM under different σ for RPCGNF-OAMNHA-CT and NF-OAMNHA-CT techniques.

Table 3: Comparison of Denoising SSIM

σ	Cameraman		Bikes	
	NF-OAMNHA-CT	RPCGNF-OAMNHA-CT	NF-OAMNHA-CT	RPCGNF-OAMNHA-CT
5	0.987	0.992	0.995	0.997
10	0.969	0.974	0.983	0.985
15	0.945	0.949	0.952	0.957
20	0.899	0.905	0.917	0.919
25	0.879	0.884	0.869	0.871
30	0.868	0.873	0.828	0.830
σ	Ocean		Statue	
	NF-OAMNHA-CT	RPCGNF-OAMNHA-CT	NF-OAMNHA-CT	RPCGNF-OAMNHA-CT
5	0.988	0.991	0.981	0.985
10	0.961	0.964	0.957	0.961
15	0.904	0.907	0.920	0.924
20	0.869	0.872	0.891	0.895
25	0.830	0.833	0.868	0.872
30	0.809	0.8132	0.849	0.853
σ	Barbara		Lena	
	NF-OAMNHA-CT	RPCGNF-OAMNHA-CT	NF-OAMNHA-CT	RPCGNF-OAMNHA-CT
5	0.988	0.992	0.971	0.975
10	0.969	0.973	0.946	0.950
15	0.956	0.960	0.930	0.934
20	0.942	0.947	0.913	0.917
25	0.920	0.924	0.899	0.903
30	0.914	0.918	0.887	0.891
σ	Coinsfountain		Lighthouse	
	NF-OAMNHA-CT	RPCGNF-OAMNHA-CT	NF-OAMNHA-CT	RPCGNF-OAMNHA-CT
5	0.989	0.992	0.979	0.983
10	0.959	0.963	0.950	0.954
15	0.924	0.927	0.930	0.934
20	0.877	0.881	0.883	0.887
25	0.829	0.834	0.870	0.874
30	0.797	0.801	0.841	0.846
σ	Stream			
	NF-OAMNHA-CT		RPCGNF-OAMNHA-CT	
5	0.996		0.998	
10	0.975		0.979	
15	0.916		0.920	
20	0.845		0.849	
25	0.781		0.785	
30	0.725		0.729	

Table 3 shows that the RPCGNF-OAMNHA-CT-based image denoising technique achieves higher SSIM compared with the NF-OAMNHA-CT technique. For case, when the statue with $\sigma = 5$ is considered for analysis, the SSIM of RPCGNF-OAMNHA-CT technique is 0.41% increased than the NF-OAMNHA-CT technique.

V. CONCLUSION

In this article, RPCGNF-OAMNHA-CT technique is proposed for removing the noisy pixels from the images and reconstructing the noise-free images. In this technique, the images considered in the CT domain are given to the recurrent mechanism based PCGNF edge detector for segmenting and extracting the edge regions and homogeneous texture regions. The main aim of applying recurrent mechanism is creating the PCGNF system for edge-preserving segmentation that learns the parameters used in the segmentation with high efficiency and speeding up the convergence. So, the edge regions and homogeneous textures are synchronously segmented as noisy pixels until either the PCGNF converges to the maximum accuracy of segmentation or a termination criterion is reached. Moreover, OAMNHA is applied on each segmented regions to remove the noisy pixels and obtain the noiseless images precisely. Finally, the experimental results proved that the RPCGNF-OAMNHA-CT technique has maximum PSNR, SSIM and minimum MAE than the NF-OAMNHA-CT technique for image denoising.

REFERENCES

1. F. Hosotani, Y. Inuzuka, M. Hasegawa, S. Hirobayashi and T. Misawa, "Image Denoising With Edge-Preserving and Segmentation Based on Mask NHA," IEEE Trans. Image Process., vol. 24, no. 12, pp. 6025-6033, 2015.
2. K. Indupriya and G. P. R. Kumar, "An Optimum Adaptive Parameterized Mask NHA Based Image Denoising," Int. J. Eng. Technol., vol. 9, no. 3, pp. 2389-2399, 2017.
3. A. S. Vijendran and K. Indupriya, "Image Denoising by Optimum Adaptive Parameterized Mask NHA in Various Frequency Domains," Int. J. Pure Appl. Math., vol. 119, no. 18, pp. 3405-3413, 2018.
4. K. Indupriya and A. S. Vijendran, "An enhancement of edge preservation in OAMNHA denoising using texture boundaries," in Kalasalingam Global Conference, International Conference on Sustainable Development, 2019.
5. X. Y. Wang, Y. C. Liu, N. Zhang, C. J. Wu and H. Y. Yang, "An edge-preserving adaptive image denoising," Multimed. Tools Appl., vol. 74, no. 24, pp. 11703-11720, 2015.
6. X. Fu, Y. Wang, L. Chen and J. Tian, "An image despeckling approach using quantum-inspired statistics in dual-tree complex wavelet domain," Biomed. Signal Process. Control, vol. 18, pp. 30-35, 2015.
7. M. B. Abdallah, J. Malek, A. T. Azar, H. Belmabrouk, J. E. Monreal and K. Krissian, "Adaptive noise-reducing anisotropic diffusion filter," Neural Comput. Appl., vol. 27, no. 5, pp. 1273-1300, 2016.
8. J. Xu, Y. Jia, Z. Shi and K. Pang, "An improved anisotropic diffusion filter with semi-adaptive threshold for edge preservation," Signal Process., vol. 119, pp. 80-91, 2016.
9. H. K. Rafsanjani, M. H. Sedaaghi and S. Saryazdi, "An adaptive diffusion coefficient selection for image denoising," Digit. Signal Process., vol. 64, pp. 71-82, 2017.
10. V. Fedorov and C. Ballester, "Affine non-local means image denoising," IEEE Trans. Image Process., vol. 26, no. 5, pp. 2137-2148, 2017.
11. H. R. Shahdoosti and S. M. Hazavei, "Image denoising in dual contourlet domain using hidden Markov tree models," Digit. Signal Process., vol. 67, pp. 17-29, 2017.
12. F. Guo, C. Zhang and M. Zhang, "Edge-preserving image denoising," IET Image Process., vol. 12, no. 8, pp. 1394-1401, 2018.
13. http://live.ece.utexas.edu/research/quality/subjective.htm

AUTHORS PROFILE

K. Indupriya is a student of Sri Ramakrishna College of Arts and Science, Coimbatore. Currently, she is pursuing a Ph.D degree in the Department of Computer Science and has teaching and development experience of 7 years. Her area of interest includes Digital Image Processing and Data Mining.

Dr. Anna Saro Vijendran is the Dean in the School of Computing, Sri Ramakrishna College of Arts and Science (formerly SNR Sons College), Coimbatore. Her research interests are in the fields of Image Processing, Artificial Neural Networks, Computer Networks, Data and Image Mining. As on date, 77 number of her research papers have been published in various Journals (UGC Approved, Scopus, SCI). In addition, she has presented 52 research articles in National and International Conferences. She is a Member of the Computer Society of India. She has been a Reviewer and Programme Committee member in International Conferences conducted in various countries.